Reconstruction Algorithm for Fan Beam with a Displaced Center-of-Rotation

GRANT T. GULLBERG, MEMBER, IEEE CARL R. CRAWFORD, MEMBER, IEEE AND BENJAMIN M. W. TSUI

Abstract—**A convolutional backprojection algorithm is derived for a fan beam geometry that has its center-of-rotation displaced from the midline of the fan beam. In single photon emission computed tomography (SPECT), where a transaxial converging collimator is used with a rotating gamma camera, it is difficult to precisely align the collimator so that the mechanical center-of-rotation is colinear with the midline of the fan beam. A displacement of the center-of-rotation can also occur in X-ray CT when the X-ray source is mispositioned. Standard reconstruction algorithms which directly filter and backproject the fan beam data without rebinning into parallel beam geometry have been derived for a geometry having its center-of-rotation at the midline of the fan beam. However, in the case of a misalignment of the center-of-rotation, if these conventional reconstruction algorithms are used to reconstruct the fan beam projections, structured artifacts and a loss of resolution will result. We illustrate these artifacts with simulations and demonstrate how the new algorithm corrects for this misalignment. We also show a method to estimate the parameters of the fan beam geometry including the shift in the center-of-rotation.**

I. Introduction

FAN beam reconstruction algorithms were derived based on the assumption that the mechanical center-of-rotation is colinear with the the midline of the fan beam [1]. This type of scanner is depicted in Fig. 1. In some situations it is not possible to align the midline with the mechanical center-of-rotation. Fig. 2 depicts a scanner in which the center-of-rotation is displaced from the midline of the fan beam. Misalignment can occur in single photon emission computed tomography (SPECT) when a fan beam collimator is used with a rotating gamma camera [2]–[4] or in X-ray CT when the X-ray source is mispositioned.

In SPECT imaging a converging collimator is used to increase the sensitivity over that of a parallel hole collimator without sacrificing resolution by mapping the emitting organ onto a larger portion of the detector. The collimator holes in the transverse reconstructed image plane are tapered and are designed to converge to the same focal point. The holes themselves are formed from corrugated sheets of lead that are glued together and stacked one upon the other. This gives holes which converge in each transaxial plane and are straight and parallel in the longitudial direction. The collimated projection events are detected using a flat NaI crystal with its associative electronics. The fan beam projections are digitized with equal spacing along the line *AB* shown in Fig. 2.

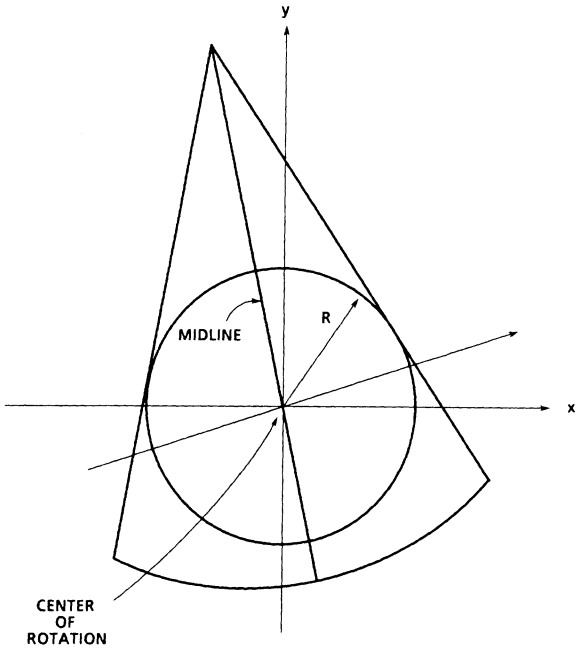

Fig. 1. Ideal fan beam geometry for a curved detector.

In designing and constructing a converging collimator, it may be difficult to align the collimator holes with the mechanical center-of-rotation as is depicted in Fig. 2. In some cases it may happen that the collimator holes have completely different focal points. It is also possible that the misalignment is a function of angle. It has been our experience [4], that the latter two cases produce variations that are less than can be detected by the resolution of the gamma camera. In this paper we assume that all collimator holes focus to a single point and that the misalignment is constant over angle.

Third-generation CT scanners use a curved detector arrangement where the detectors are placed at equal intervals on an arc concentric with the source. An example of

Manuscript received June 20, 1985; revised November 21, 1985. This work was done while the first author was with the General Electric Company, Medical Systems Business Group, Applied Science Laboratory, Milwaukee, WI 53201.

G. T. Gullberg is with the Department of Radiology, University of Utah, Salt Lake City, UT 84132.

C. R. Crawford is with the General Electric Company, Medical Systems Business Group, Applied Science Laboratory, Milwaukee, WI 53201.

B. M. W. Tsui is with the Department of Radiology and Curriculum in Biomedical Engineering, University of North Carolina, Chapel Hill, NC 27514.

IEEE Log Number 8407243.

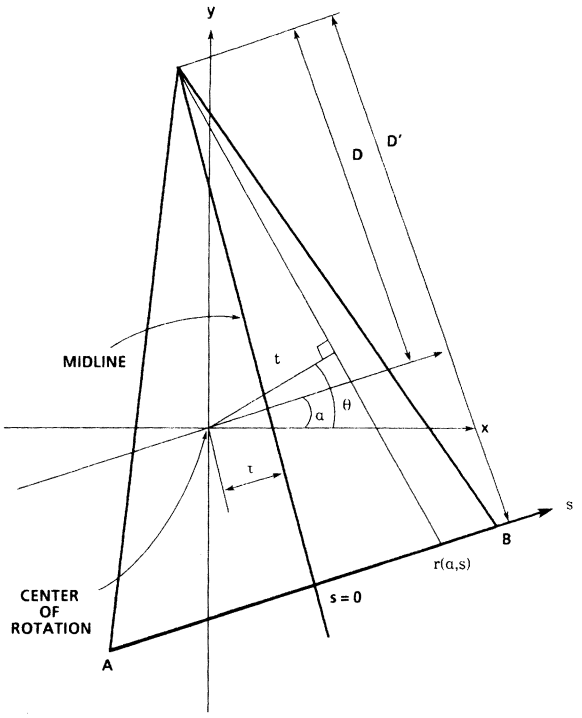

Fig. 2. Fan beam geometry with a displaced center-of-rotation for a flat detector.

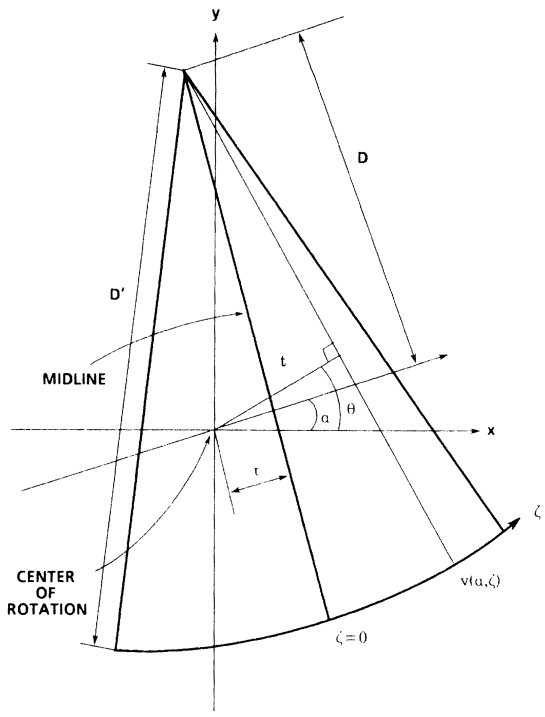

Fig. 3. Fan beam geometry with a displaced center-of-rotation for a curved detector.

this geometry is shown in Fig. 1. Here the center-of-rotation is colinear with the midline of the fan beam. The case where there is a displaced center-of-rotation is depicted in Fig. 3. The common terminology for the curved detector arrangement is that the data are sampled with equal angles, where as for the flat detector the data are sampled with equal spacing.

When data from a misaligned system are reconstructed without taking into consideration the shift in the midline, there will be a loss of resolution for 360 degree reconstructions [5]. For *halfscans* [6], which are reconstructions from projections sampled over 180 degrees plus the fan angle, structured artifacts will result [7]. In the parallel beam case, it is possible to simply shift the projection prior to processing in order to account for the new center-of-rotation [8]. However, the fan beam case for a flat detector cannot be corrected by a simple shift, unless of course the fan beam projections are rebinned [9] into parallel beam projection sets. Rebinning, however, is computationally expensive and it degrades resolution.

Fan beam algorithms for geometries other than the standard configuration are also available. Horn described reconstruction algorithms for arbitrary fan beam geometries for the case when the midline is colinear with the center-of-rotation [10]. Weinstein described a scanner where the focus-to-center distance is a function of rotation angle [11]. However, the results of these papers are not extendable to the misaligned scanner described here.

In this paper a convolutional backprojection algorithm is derived which corrects for the misalignment of the fan beam for both a flat detector and a curved detector. Simulations are given which show the effects of the shift and demonstrate the new algorithm's ability to correct for the misalignment. A method is also developed to estimate the parameters of the fan beam geometry including the shift in the center-of-rotation.

II. Derivation for Flat Detector

The function $f(x, y)$ is used to denote the cross section of an object to be reconstructed from its projections. The function $f(x, y)$ may be the distribution of the linear attenuation coefficients for X-ray CT or the radiopharmaceutical concentration for SPECT. It is assumed that the object is zero outside of a circle of radius R. A parallel projection of $f(x, y)$, $p(\theta, t)$ is the collection of line integrals through $f(x, y)$ along the paths given by

$$t = x \cos \theta + y \sin \theta \tag{1}$$

for a fixed value of θ.

A polar coordinate version $f(r, \phi)$, of the original function $f(x, y)$, can be reconstructed from its projections using Radon's inversion relationship

$$f(r, \phi) = 1/(4\pi^2) \int_0^{2\pi} \int_{-R}^{R} p'(\theta, t)/ \cdot [r \cos (\theta - \phi) - t]\, dt\, d\theta \tag{2}$$

where p' is the partial derivative of p with respect to t. The integral over t is the composite of the derivative and Hilbert transform operators [12]. It can be shown that $f(r, \phi)$ can be reconstructed using the following integral equation [12]:

$$f(r, \phi) = \int_0^{2\pi} \int_{-R}^{R} p(\theta, t) h(r \cos (\theta - \phi) - t)\, dt\, d\theta \tag{3}$$

where $h(t)$ is the inverse Fourier transform of $|\omega|/2$ and $h(t)$ satisfies

$$h(at) = h(t)/a^2. \tag{4}$$

Consider the fan beam geometry depicted in Fig. 2 in which the midline is displaced from the center-of-rotation by τ. A fan beam projection in this system is denoted by $r(\alpha, s)$. It can be seen from Fig. 2, that the fan beam and parallel projections are related as follows:

$$p(\theta, t) = r(\alpha, s) \tag{5}$$

for

$$t = (s + \tau)Z \tag{6}$$

$$\theta = \alpha + \tan^{-1}(s/D) \tag{7}$$

where, for mathematical purposes, it has been assumed that the focus-to-detector distance D' is equal to the focus-to-center distance D and

$$Z = D[s^2 + D^2]^{-1/2}. \tag{8}$$

Using (6) and (7) the reconstruction formula given by (3) for the parallel projection case can be implemented in the fan beam (α, s) space. The Jacobian for this transformation is

$$J(s, \alpha) = (D^2 - \tau s)Z^3D^{-2}. \tag{9}$$

Using (6), (7), and (9), we arrive at

$$f(r, \phi) = \int_0^{2\pi} \int_{-W}^{W} r(\alpha, s)(D^2 - \tau s)Z^3D^{-2} \cdot h(r \cos[\tan^{-1}(s/D) + \alpha - \phi] - (s + \tau)Z)\, ds\, d\alpha \tag{10}$$

where W is the value of s for which $r(\alpha, s) = 0$ with $|s| > W$ in all the projections. The variable W is determined by letting $t = R$ in (6) and solving for s

$$W = (DR(\tau^2 + D^2 - R^2)^{1/2} - \tau D^2)/(D^2 - R^2). \tag{11}$$

The argument of the filter h in (10),

$$(r \cos[\tan^{-1}(s/D) + \alpha - \phi] - (s + \tau)Z), \tag{12}$$

can be reduced to

$$UZ(s' - s) \tag{13}$$

where

$$s' = [rD \cos(\alpha - \phi) - \tau D]/[r \sin(\alpha - \phi) + D] \tag{14}$$

$$U = [r \sin(\alpha - \phi) + D]/D. \tag{15}$$

Using (13) and (4) we see that

$$h(r \cos[\tan^{-1}(s/D) + \alpha - \phi] - (s + \tau)Z) = h(s' - s)/(UZ)^2. \tag{16}$$

The following is obtained when (16) is substituted into (10):

$$f(r, \phi) = \int_0^{2\pi} q(\alpha, s')/U^2\, d\alpha \tag{17}$$

where

$$q(\alpha, s') = \int_{-W}^{W} r(\alpha, s) \cdot [(D - \tau s/D)/(D^2 + s^2)^{1/2}]\, h(s' - s)\, ds. \tag{18}$$

Equation (17) represents a filtered backprojection algorithm for equal spaced fan beam projections that have been collected with a shift in the center of rotation.

The following is a summary of the fan beam reconstruction algorithm.

1) Multiply each fan beam projection $r(\alpha, s)$ by $[(D - \tau s/D)/(D^2 + s^2)^{1/2}]$.

2) Convolve each weighted projection with $h(s)$.

3) For each pixel in the reconstructed image and for each filtered projection, determine the value of the filtered projection at s' given in (14) and weight this value by U^{-2} given in (15). Add the weighted filtered projection value into the reconstructed image.

It should be noted that the adaptation of the analytic reconstruction algorithms to actual machine implementations can be done only with the introduction of approximations. The approximations deal with sampling considerations with regard to the kernel used to filter the weighted projection data and the conversion of the sampled filtered projections to continuously filtered projections [13]. In practice, the convolution indicated in (18) is performed using fast Fourier transform (FFT) operations incorporating the FFT of the filter $h(s)$ and the FFT of the sampled projections $r(\alpha, s)$. Because of noise and aliasing, the filter is rolled-off using a suitable window. Convolutional fan beam algorithms cannot be exactly derived if a window is used. However, because the window can be exactly incorporated into convolutional parallel beam reconstruction algorithms, it has been correctly assumed that the use of a window will not adversely affect the quality of images obtained with the fan beam algorithm. The equation given in (17) can be combined with material found in [6] to obtain a *halfscan* reconstruction algorithm for projections collected with a displaced center-of-rotation.

III. Derivation for Curved Detector

The curved detector geometry shown in Fig. 3 samples each projection at equal angular intervals in contrast to the flat detector geometry in Fig. 2 which samples at equal spatial intervals. For the curved detector geometry at the projection angle α the samples will be located at angles ζ/D' where ζ is the coordinate along the curved detector shown in Fig. 3. A fan beam projection in this system is denoted by $v(\alpha, \zeta)$. It can be seen from Fig. 3 that the fan beam and parallel projections are related as follows:

$$p(\theta, t) = v(\alpha, \zeta) \tag{19}$$

for

$$t = D \sin(\zeta/D) + \tau \cos(\zeta/D) \tag{20}$$

$$\theta = \alpha + \zeta/D \tag{21}$$

where, for mathematical purposes, it has been assumed that the focus-to-detector distance D' is equal to the focus-to-center distance D.

Using (20) and (21) the reconstruction formula given by (3) can be implemented in the fan beam (α, ζ) space for a curved detector. The Jacobian for this transformation is

$$J(\zeta, \alpha) = \cos(\zeta/D) - (\tau/D)\sin(\zeta/D). \tag{22}$$

Using (20), (21), and (22), we arrive at

$$f(r, \phi) = \int_0^{2\pi} \int_{-X}^{X} v(\alpha, \zeta)[\cos(\zeta/D) - (\tau/D)\sin(\zeta/D)] \cdot h(r\cos[\zeta/D + \alpha - \phi] - D\sin(\zeta/D) - \tau\cos(\zeta/D))\, d\zeta\, d\alpha \tag{23}$$

where

$$X = D\tan^{-1}(W/D) \tag{24}$$

and W is given in (11).

The argument of the filter h in (23),

$$r\cos[\zeta/D + \alpha - \phi] - D\sin(\zeta/D) - \tau\cos(\zeta/D), \tag{25}$$

can be reduced to

$$E\sin(\zeta'/D - \zeta/D) \tag{26}$$

where

$$E = ([r\cos(\alpha - \phi) - \tau]^2 + [r\sin(\alpha - \phi) + D]^2)^{1/2} \tag{27}$$

$$\zeta' = D\tan^{-1}[(r\cos(\alpha - \phi) - \tau)/(r\sin(\alpha - \phi) + D)]. \tag{28}$$

Using (4) and (26) we see that

$$h(r\cos[\zeta/D + \alpha - \phi] - D\sin(\zeta/D) - \tau\cos(\zeta/D)) = h(D\sin(\zeta'/D - \zeta/D))D^2/E^2. \tag{29}$$

The following is obtained when (29) is substituted into (23):

$$f(r, \phi) = \int_0^{2\pi} g(\alpha, \zeta')D^2/E^2\, d\alpha \tag{30}$$

where

$$g(\alpha, \zeta') = \int_{-X}^{X} v(\alpha, \zeta)\,[\cos(\zeta/D) - (\tau/D)\sin(\zeta/D)] \cdot h(D\sin(\zeta'/D - \zeta/D))\, d\zeta. \tag{31}$$

This gives a filtered backprojection algorithm for equal-angle fan beam projections that have been collected with a curved detector and a shift in the center-of-rotation.

The following is a summary of the fan beam reconstruction algorithm.

1) Multiply each fan beam projection $v(\alpha, \zeta)$ by $\cos(\zeta/D) - (\tau/D)\sin(\zeta/D)$.

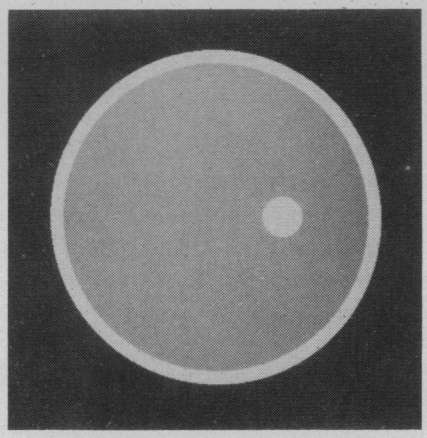

Fig. 4. Phantom used in the computer simulation studies.

TABLE I
DESCRIPTION OF THE ELLIPSES USED TO CONSTRUCT THE PHANTOM SHOWN IN FIG. 4.

Ellipse	Origin X	Origin Y	Semi-Major Axes X	Semi-Major Axes Y	Rotation Angle	Density
1	0 mm	0 mm	25 mm	25 mm	0	1532 HU
2	0	0	23	23	0	−532
3	10	0	3	3	0	266

2) Convolve each weighted projection with $h(D\sin[\zeta/D])$.

3) For each pixel in the reconstructed image and for each filtered projection, determine the value of the filtered projection at ζ' given in (28) and weight this value by D^2/E^2 where E is given in (27). Add the weighted filtered projection value into the reconstructed image.

For the curved detector case it would be a simple matter to rotate the ζ coordinate system so that the midline of the fan beam goes through the center-of-rotation. Then conventional convolutional algorithms could be used (i.e., $\tau = 0$). However, the distance to the center-of-rotation would not equal the distance D shown in Fig. 3. If filtered backprojection algorithms are implemented in hardware, parameters such as D may be hardwired. If the algorithm is implemented as derived here, then it would not be necessary to modify any hardware for shifts in the center-of-rotation.

IV. Computer Simulation Results

A computer program was written to generate the X-ray line-integral data for the phantom shown in Fig. 4. A description of the ellipses used to construct the phantom can be found in Table I. An equal-angle configuration (see Fig. 3) with a point source and a point detector was simulated with a focus-to-center distance D of 630 mm, a focus-to-detector distance D' of 1100 mm, and a detector spacing of 0.2 mm. Data were generated for 1000 projections with 768 samples per projection.

Fig. 5 shows a normal 512 × 512 reconstruction, with a pixel size of 0.125 mm, of projection data generated without a shift in the center-of-rotation. Fig. 6 is the same

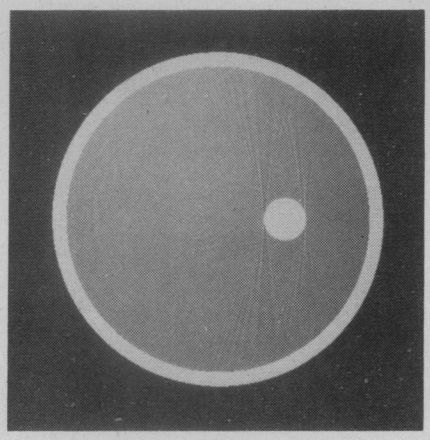

Fig. 5. Normal reconstruction of the phantom.

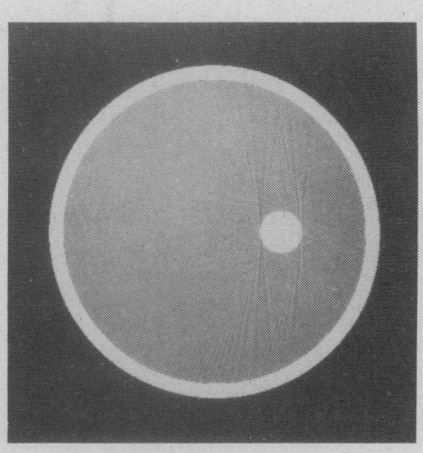

Fig. 6. *Halfscan* reconstruction of the phantom.

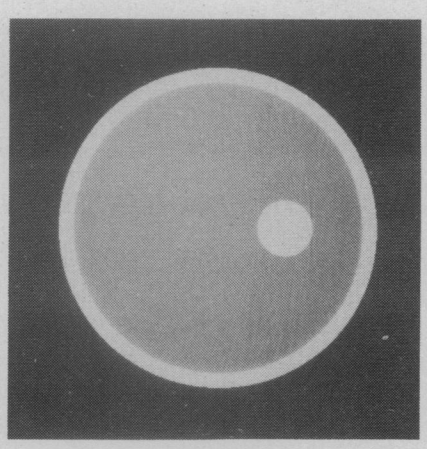

Fig. 7. Normal reconstruction of shifted data without compensation for the shift.

as Fig. 5 but now a *halfscan* reconstruction algorithm was used. The subtle streaks and other structured artifacts are due to aliasing and an insufficient number of views.

Line integral data were then generated for the case when the center-of-rotation was shifted by 1 mm. The normal and *halfscan* reconstructions of the data, without correcting for the shift in the center-of-rotation, are shown in Figs. 7 and 8, respectively. Structured artifacts are clearly seen in Fig. 8. The loss of resolution that occurs when

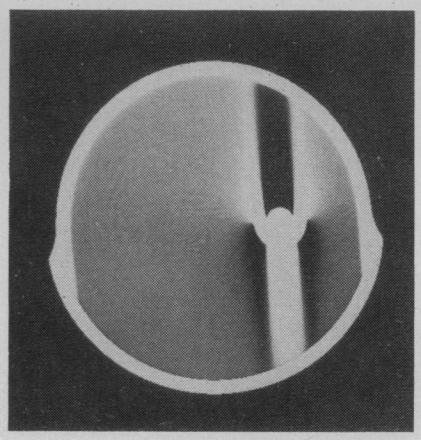

Fig. 8. *Halfscan* reconstruction of shifted data without compensation for the shift.

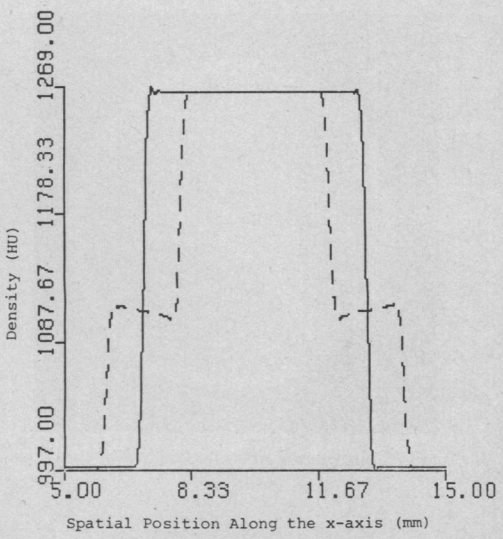

Fig. 9. Cross sections through the small off-center object from Fig. 5 (solid line) and from Fig. 7 (dashed line).

shifted data are reconstructed without compensation can be seen more clearly in a density cross section through the small off-center object in the phantom. Fig. 9 shows the cross sections through this object from Fig. 5 and from Fig. 7.

Finally, the normal and *halfscan* reconstructions of the data, with correction for the shift in the center-of-rotation, are shown in Figs. 10 and 11, respectively. It is clear that the new reconstruction algorithm corrects for a shift in the center-of-rotation.

V. Estimation of Fan Beam Parameters

In parallel beam systems it is relatively easy to take calibrating measurements to determine the shift in the center-of-rotation. This is done by using a point source and taking complementary views 180 degrees apart. The projection of the center-of-rotation onto the image plane is determined by summing the centroids of the projected point source and dividing by two. A small source of radioactivity is used in SPECT as the point source and a pin of highly attenuating material is used in X-ray CT.

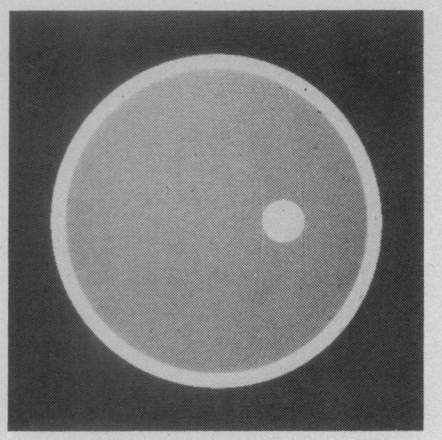

Fig. 10. Normal reconstruction of shifted data with compensation for the shift.

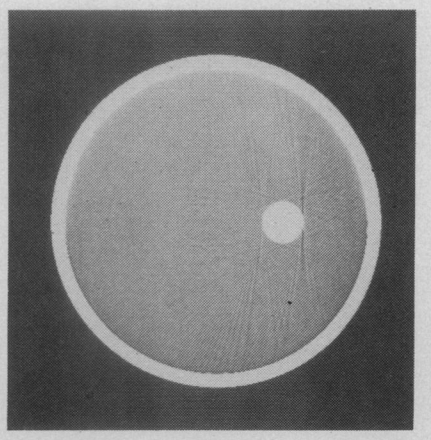

Fig. 11. *Halfscan* reconstruction of shifted data with compensation for the shift.

In this section we show a method for measuring the parameters of the fan beam geometry shown in Fig. 12. The parameters are the displaced center-of-rotation τ, focus-to-center distance D, focus-to-detector distance D', and the location c, of the projection of the focus onto the detector. For the purpose of estimating the parameters, the projection coordinate ξ denotes the distance from the edge of the measurable detector region. Mathematically, we use

$$f(x, y) = \delta(x - x_0)\,\delta(y - y_0) \tag{32}$$

for a point source located at (x_0, y_0) to develop a relationship between the parameters of the fan beam geometry shown in Fig. 12 and something we can measure, namely, the centroids of the projected point source.

The fan beam projection operator [14] for the geometry in Fig. 12 is

$$R(\alpha, \xi) = \int_{-\infty}^{\infty}\int_{-\infty}^{\infty} f(x, y) \cdot \delta((\xi - c)\,(x \sin\alpha - y\cos\alpha + D)/D' - x\cos\alpha - y\sin\alpha + \tau)\,dx\,dy. \tag{33}$$

The projections of the point source are obtained by substituting (32) into (33)

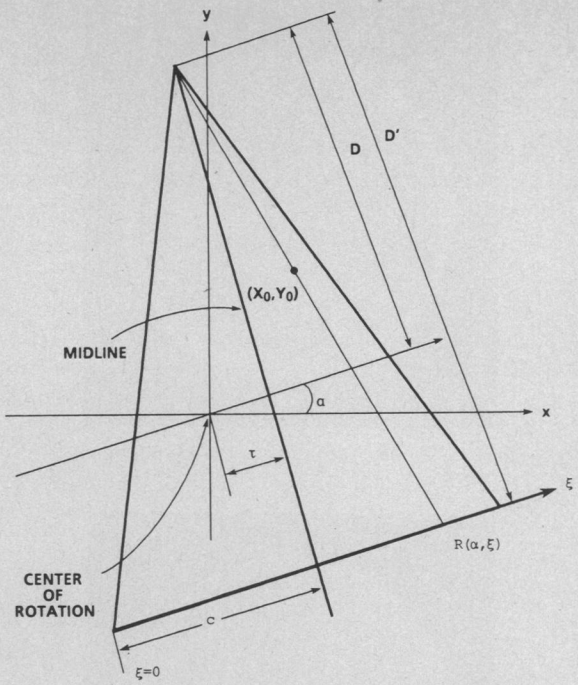

Fig. 12. The estimated parameters for the fan beam geometry.

$$R(\alpha, \xi) = \delta((\xi - c)(x_0 \sin\alpha - y_0\cos\alpha + D)/D' - x_0\cos\alpha - y_0\sin\alpha + \tau). \tag{34}$$

For the angle α, the centroid of a projection is $\rho(\alpha)$ defined by

$$\rho(\alpha) = \int_{-\infty}^{\infty} R(\alpha, \xi)\xi\,d\xi \Big/ \int_{-\infty}^{\infty} R(\alpha, \xi)\,d\xi. \tag{35}$$

Substituting (34) into (35) and integrating, we obtain

$$\rho(\alpha) = D'(x_0\cos\alpha + y_0\sin\alpha - \tau)/(x_0\sin\alpha - y_0\cos\alpha + D) + c. \tag{36}$$

The result in (36) gives an expression for the projected centroid of a point source in terms of the fan beam parameters. This suggests a method to estimate the geometry of a fan beam system. In practice, a point source is placed in the field of view of the scanner. Projections of the point source are collected and the centroid $\hat{\rho}_i$ is calculated for each angle α_i using (35). The parameters of the fan beam geometry can be estimated by minimizing the chi-square function

$$\chi^2(x_0, y_0, D, D', c, \tau) = \sum_i [\hat{\rho}_i - \rho(\alpha_i)]^2 \tag{37}$$

where $\rho(\alpha_i)$ is given in (36). The process of minimizing (37) to determine estimates of the fan beam geometry is a nonlinear estimation problem which can be solved using the Marquardt algorithm [15].

VI. Summary

A method has been shown for determining and correcting for shifts in the center-of-rotation of a fan beam computed tomographic system. The projection data are pre-

processed by multiplying by weighting factors which incorporate the displacement of the center-of-rotation. The modified projections are filtered and then backprojected correctly into a coordinate system whose center-of-rotation is displaced from the midline of the fan beam. The algorithm has been verified with computer simulations and has been implemented on a SPECT system showing good results with both patient and phantom studies [4].

Acknowledgment

The authors would like to thank D. Snider for preparing the line drawings.

References

[1] G. T. Herman and A. Naparstek, "Fast image reconstruction based on a Radon inversion formula appropriate for rapidly collected data," *SIAM J. Appl. Math.*, vol. 33, pp. 511-533, Nov. 1977.

[2] R. J. Jaszczak, L. T. Chang, and P. H. Murphy, "Single photon emission computed tomography using multislice fan beam collimator," *IEEE Trans. Nucl. Sci.*, vol. NS-26, pp. 610-618, Feb. 1979.

[3] C. B. Lim, L. T. Chang, and R. J. Jaszczak, "Performance analysis of three camera configurations for single photon emission computed tomography," *IEEE Trans. Nucl. Sci.*, vol. NS-27, pp. 559-568, Feb. 1980.

[4] B. M. W. Tsui, G. T. Gullberg, E. R. Edgerton, D. R. Gilland, J. R. Perry, and W. H. McCartney, "The design and clinical utility of a fan beam collimator for SPECT imaging of the head," *J. Nucl. Med.*, submitted for publication.

[5] M. Kijewski and P. Judy, "The effects of misregistration of the projections on spatial resolution of CT scanners," *Med. Phys.*, vol. 10, pp. 169-175, Mar. 1983.

[6] D. L. Parker, "Optimal short-scan convolution reconstruction or fan beam CT," *Med. Phys.*, vol. 9, pp. 254-257, Apr. 1982.

[7] L. A. Shepp, S. K. Hilal, and R. A. Schultz, "The tuning fork artifact in computed tomography," *Comput. Graphics Image Processing*, vol. 10, pp. 246-255, 1979.

[8] M. Dennis, R. Waggener, W. McDavid, W. Payne, and V. Sank, "Preprocessing X-ray transmission data in CT scanning," *Opt. Eng.*, vol. 16, pp. 6-10, Jan. 1977.

[9] P. Dreike and D. P. Boyd, "Convolution reconstruction of fan-beam projections," *Comput. Graphics Image Processing*, vol. 5, pp. 459-469, 1976.

[10] B. K. P. Horn, "Fan beam reconstruction methods," *IEEE Proc.* vol. 67, pp. 1616-1623, Dec. 1979.

[11] F. S. Weinstein, "Formation of images using fan beam scanning and noncircular source motion," *J. Opt. Soc. Amer.*, vol. 70, pp. 931-935, Aug. 1980.

[12] A. Rosenfeld and A. C. Kak, *Digital Picture Processing—Second Edition*. New York: Academic, 1982, vol. 1, ch. 8.

[13] C. R. Crawford and A. C. Kak, "Aliasing artifacts in computerized tomography," *Appl. Opt.*, vol. 18, pp. 3704-3711, Nov. 1979.

[14] G. T. Gullberg, "The reconstruction of fan-beam data by filtering the back-projection," *Comput. Graphics Image Processing*, vol. 10, pp. 30-47, 1979.

[15] D. W. Marquardt, "An algorithm for least-squares estimation of nonlinear parameters," *SIAM J. Appl. Math.*, vol. 11, pp. 431-441, June 1963.